IMPROVING TIE POINT EXTRACTION BY ANISOTROPIC DIFFUSION

R. Schmidt[a], C. Heipke[a], G. Neukum[b] and the HRSC Co-Investigator Team

[a]Institute of Photogrammetry and GeoInformation, Leibniz University of Hannover, Nienburger Str. 1, D-30167 Hannover, Germany, schmidt@ipi.uni-hannover.de
[b]Institute of Geosciences, Remote Sensing of the Earth and Planets, Freie Universität Berlin, Malteserstr. 74-100, D-12249 Berlin, Germany, gneukum@zedat.fu-berlin.de

Commission IV, WG IV/7

ABSTRACT:

Mars Express is in orbit for over two years and has returned more than 1.000 image strips to earth taken by the multiple line scanner camera HRSC (High Resolution Stereo Camera). The three-dimensional position of the spacecraft is continually determined by the Flight Dynamics Team (FDT) at ESOC (European Space Operations Centre) in Darmstadt, Germany. The HRSC experiment with its multiple stereo lines is designed with the goal in mind to improve these nominal values of exterior orientation by means of photogrammetric techniques. First, tie points are determined automatically via image matching. After that a bundle adjustment is carried out to improve the exterior orientation.
Unfortunately image quality is frequently degraded by noise from the incoming signal and camera electronics and by compression artefacts. In case of a low signal-to-noise ratio it is difficult or even impossible to derive correct and an adequate amount of tie points with image matching techniques. This paper deals with image restoration using anisotropic diffusion to improve tie point extraction. The results of the matching, the distribution of the tie points in the images and the achieved accuracy are presented and evaluated on the basis of some selected Mars Express orbits.

1. INTRODUCTION

Mars Express is in orbit for over two years and has returned more than 1 000 image strips to earth taken by the multiple line scanner camera HRSC (High Resolution Stereo Camera). The three-dimensional position of the spacecraft is determined by the Flight Dynamics Team (FDT) at ESOC (European Space Operations Centre) in Darmstadt, Germany from ranging and Doppler shift measurements. An onboard star tracker is used to control the spacecraft's attitude (and thus the pointing of the body-fixed camera). These values result in a three-dimensional position and attitude of the spacecraft over time (termed "exterior orientation" (EO) in classical photogrammetry). Unfortunately, these parameters are sometimes poorly constrained but the HRSC experiment with its multiple stereo lines is designed with the goal in mind to improve these nominal values of exterior orientation by means of photogrammetric techniques. This is accomplished in two steps. First, a large number of tie points between the multiple stereo strips are extracted via digital image matching (DIM). Then, a bundle adjustment (BA) is performed to correct the EO, using the collected tie points as observations for the unknown EO parameters.

The tie points are determined automatically at the Institute of Photogrammetry and GeoInformation (IPI), University of Hannover (Heipke et al., 2004). The subsequent BA is carried out at Department Photogrammetry and Remote Sensing (FPF), Technical University Munich (Ebner et al., 2004). The remaining processing like digital terrain model (DTM) and orthophoto generation is done at Deutsches Zentrum für Luft- und Raumfahrt e.V. (DLR) in Berlin Adlershof (Scholten et al., 2005). Until now the first 750 orbits have been investigated by IPI and FPF and 544 of them have been processed successfully.

In 165 orbits it was possible to improve the stereo ray intersections via BA but the amount of tie points was not sufficient to fit the point cloud of the tie points to MOLA (Zuber et al. 1992). This means that an improvement of the absolute position of the camera with respect to the Mars fixed coordinate system did not succeed. In case of the remaining 41 orbits no result for the BA could be achieved because of very degraded imagery.

The main reason for generating too few tie points – and therefore resulting in an unsuccessful BA – comes from an unstable matching process caused by a too low signal-to-noise ratio in the imagery. In addition to noise there is another effect which can degrade the quality of the imagery. Because of a limited data rate between the spacecraft and earth it is not possible to transmit uncompressed imagery. Hence, onboard the spacecraft the images are compressed on-line with a DCT (Discrete Cosine Transformation) approach known from the JPEG algorithm. The compression ratio is adapted automatically depending on the local spatial frequency of the image which is influenced by local contrast and texture. So, for areas in the image with low contrast and low texture a high compression ratio is attained. In this case visible artefacts appear in the images which disturb image matching.

The objective of reducing image noise and compression artefacts is to improve the reliability and completeness of the feature extraction and the image matching in areas with a low signal-to-noise ratio by enhancing contrast and edges and smoothing homogeneous regions. Similar investigations for the derivation of DTMs (Digital Terrain Models) have been reported in Gwinner et al. (2005).

In section two of this paper a brief introduction to anisotropic diffusion is given and the applied algorithm is presented. In section three the test data is described and the results of tie point matching derived from selected orbits are shown and discussed. The last section summarises the results and gives an outlook on how to further improve the processing. A detailed description of the Mars Express Mission and the HRSC camera is given in Chicarro et al. (2004) and Neukum et al. (2004).

2. ANISOTROPIC DIFFUSION

2.1 Noise

Several independent noise processes are overlaid in the image. However, it is a complex task to separate the different noise sources and they also vary with the intensity function of the image. Noise can be induced by the input signal (photon noise) or by the instrument electronics. If the detector receives only a weak signal or the atmosphere weakens the wanted signal from the surface of Mars this results in a low signal-to-noise ratio. Also unfavourable lightning can influence the imaging conditions in a negative way. The consequence is low image contrast especially in areas with low texture overlaid with noise. The signal-to-noise ratio of the input signal can only be raised by collecting a greater amount of photons. Unfortunately, due to limited aperture and integration time this is not possible. Additional noise can be introduced by the camera electronics, namely thermal, dark current shot noise, quantisation noise, flicker noise or stray field noise from other instruments. There is also fixed pattern noise which has been determined during the radiometric calibration of the camera and is being corrected in the radiometric preprocessing of the imagery.

2.2 Perona and Malik algorithm

The method of anisotropic diffusion can be applied to edge detection and image segmentation. In this paper it is used for image restoration. It was introduced by Perona and Malik (1990) and their starting point was the scale-space theory introduced by Witkin (1983). For two-dimensional signals (images) the linear scale-space is derived by convolving the original image $I_0(x, y)$ with a Gaussian kernel $G(x, y, t)$ of variance $t = \sigma^2$.

$$G(x, y, t) = \frac{1}{2\pi t} e^{-\frac{x^2 + y^2}{2t}} \quad (1)$$

where   x, y = spatial position
   t = artificial time parameter

The resulting linear scale-space is a family of derived signals $I(x, y, t)$ with coarser resolution.

$$I(x, y, t) = I_0(x, y) * G(x, y, t) \quad (2)$$

Equivalently, these scale-space images can be viewed as the solution of the heat equation

$$\frac{\partial I}{\partial t} = \nabla^2 I = (I_{xx} + I_{yy}) \quad (3)$$

with the initial condition $I(x, y, t_0) = I_0(x, y)$ and the gradient operator ∇. In this isotropic diffusion heat can dissipate equally in all directions in a homogeneous medium. Koenderink (1984) introduces two hypotheses for the diffusion process:

1) *Causality*: Any feature at a coarse level of resolution is required to possess a (not necessarily unique) "cause" at a finer level of resolution although the reverse need not be true. This forbids the generation of spurious details in coarser resolutions.

2) *Homogeneity and isotropy*: This hypothesis forbids space variant blurring and is only introduced for simplicity.

As shown in Witkin (1983) a major disadvantage of the second hypothesis is that Gaussian blurring results in eliminated, displaced and blurred edges which can be observed in figure 1. An edge is defined here as a semantically meaningful region boundary.

Figure 1: Position of the edges (zero crossings of the Laplacian with respect to x) through linear scale-space [adapted from Witkin (1983)].

To circumvent this drawback the second hypothesis of Koenderink (1984) is replaced in Perona and Malik (1990) by two new criteria:

1) *Immediate Localisation*: At each resolution, the region boundaries should be sharp and coincide with the semantically meaningful boundaries at that resolution.

2) *Piecewise Smoothing*: At all scales, intraregional smoothing should occur preferentially over interregional smoothing.

In isotropic diffusion the diffusion coefficient c (see eq. 4) is assumed to be a constant independent of location and direction. Perona and Malik (1990) introduced a spatially varying anisotropic diffusion coefficient $c(x, x, t)$ where heat cannot dissipate uniformly in all directions.

$$\frac{\partial I}{\partial t} = \text{div}(c(x, y, t)\nabla I) = c(x, y, t)\nabla^2 I + \nabla c \nabla I \quad (4)$$

where   div = divergence operator
   c(x, y, t) = diffusion coefficient
   ∇ = gradient operator

This anisotropic diffusion is discretised by a moving operator with a four pixel neighbourhood though also other pixel neighbourhoods (Barash, 2005) are possible:

$$I_{i,j}^{t+1} = I_{i,j}^t + \lambda(c_N \cdot \nabla_N I + c_S \cdot \nabla_S I + c_E \cdot \nabla_E I + c_W \cdot \nabla_W I) \quad (5)$$

where $I_{i,j}^{t+1}$ = new grey value

$I_{i,j}^{t}$ = current grey value

λ = weight value (0.25 for four pixel neighbourhood)

c_X = directional diffusion coefficient, subscript X indicates direction (North, South, East, West), function of the directional grey value gradient

$\nabla_X I$ = directional grey value gradients (grey value of neighbouring pixel minus current pixel)

The directional grey value gradients are calculated this way:

$$\begin{aligned}
\nabla_N I_{i,j} &\equiv I_{i-1,j} - I_{i,j} \\
\nabla_S I_{i,j} &\equiv I_{i+1,j} - I_{i,j} \\
\nabla_E I_{i,j} &\equiv I_{i,j+1} - I_{i,j} \\
\nabla_W I_{i,j} &\equiv I_{i,j-1} - I_{i,j}
\end{aligned} \qquad (6)$$

The location of edges is unknown. As a simple estimate the directional grey value gradients are used. Two functional forms for $c_x = g(\nabla_x I)$, termed "edge-stopping" function, have been introduced by Perona and Malik (1990):

1) *Exponential* form:

$$g_e(\nabla I) = e^{-\left(\frac{\|\nabla I\|}{K}\right)^2} \qquad (7)$$

2) *Inverse* form:

$$g_i(\nabla I) = \frac{1}{1 + \left(\frac{\|\nabla I\|}{K}\right)^2} \qquad (8)$$

where K = determines magnitude of the edges to be preserved and rate of diffusion

With low values of K small gradients can block diffusion, whereas high values admit diffusion in areas with relatively big gradients. The exponential form privileges high-contrast edges over low-contrast ones, the inverse form privileges wide regions over smaller ones. It is shown in Perona and Malik (1990) that using an appropriate spatially varying diffusion coefficient not only preserves edges but also sharpens them.

2.3 Robust anisotropic diffusion

A vast amount of research has been undertaken to understand the mathematical properties of anisotropic diffusion and the relations to other image restoration techniques, finding well-posed functions or developing modifications for fast implementations or special applications. A brief overview of literature can be found in Acton (2000) and in Black et al. (1998). In the latter the relations to robust statistics have been derived. It is shown that the edge-stopping function is connected to error norm and influence function (Hampel et al, 1986) of a robust estimation process. This allows to investigate the characteristics of these functions and to derive new edge-stopping functions.

The input image is considered as a piecewise constant (smooth) function which is overlaid with zero-mean Gaussian noise with small variance. This is appropriate because noise processes can be described well with Gaussian distributions. An optimal estimator for the noiseless true intensity function minimises the square of the directional differences which is equivalent to calculating the mean of the grey values of the differences. For regions containing an edge the assumption of a Gaussian distribution is no longer valid. This means that boundaries between smooth image regions can be considered as an outlier with respect to a Gaussian distribution.

Outlier detection, and therefore edge preservation, can be controlled with a suitable choice of the robust error norm. In case of Perona and Malik's exponential form (7) the underlying robust error norm is related to Leclerc (1989). The inverse form (8) is based on the Lorentzian error norm (Cauchy distribution). A more suitable error norm than the two mentioned above is Tukey's biweight function because it can suppress outliers. This function results in the following edge-stopping function:

$$g(\nabla I, \sigma) = \begin{cases} \frac{1}{2}\left[1 - (\nabla I / \sigma)^2\right]^2 & |\nabla I| \leq \sigma \\ 0 & \text{otherwise} \end{cases} \qquad (9)$$

The robust scale $\sigma(\nabla_x I)$ controls how large the gradient of the intensity function can be before it is considered to be an outlier. In Black et al. (1998) this parameter is determined automatically from the image as:

$$\begin{aligned}
\sigma_g &= 1.4826 \, \text{MAD}(\nabla I) \\
&= 1.4826 \, \text{median}_I \left[|\nabla I - \text{median}_I(|\nabla I|)| \right]
\end{aligned} \qquad (10)$$

MAD is a common abbreviation for median absolute deviation (Hampel, 1974) and the MAD of a zero-mean normal distribution with unit variance is $0.6745 = 1/1.4826$. The subscript I denotes that the median has to be calculated over the entire image. HRSC images can contain more than 300 000 lines so that the file size exceeds easily 1 GByte. To handle these huge amounts of data the calculation of the global scale σ_g is implemented using the Remedian (Rousseeuw & Bassett, 1990). Another possibility to estimate the scale is to use the standard deviation of the image.

Figure 2 shows a plot of the three presented edge-stopping functions. For the Perona-Malik Inverse function it is clearly visible that even large gradients have an influence on the diffusion because the function approaches zero asymptotically. In principle this also holds for the Exponential form albeit diffusion is reduced stronger over high-contrast edges. Only with the Robust form diffusion is stopped at a certain given scale because the function descends to zero.

An extension to this approach with a spatially varying σ is presented in Black & Sapiro (1999). This means that σ is related to the local texture resulting in stronger diffusion in areas with high texture. This is useful if only relevant edges should be extracted in highly textured areas. For the reduction of noise this is not reasonable because we assume the noise level of HRSC imagery to be equal across the whole image. Furthermore, the estimation of a local scale significantly increases the computing time. For processing huge amounts of

data like in the HRSC project this is not acceptable. Therefore, only a global scale estimate as presented in (10) is used here.
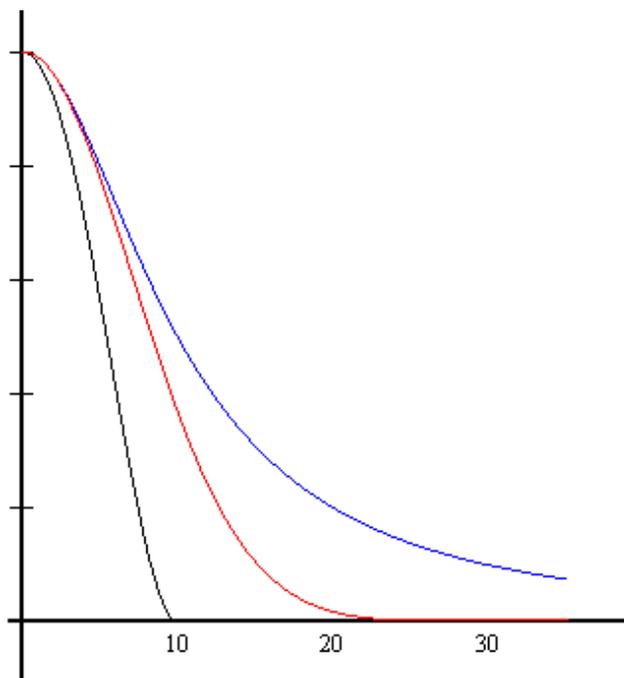
Figure 2: Plot of the three presented edge-stopping functions
(from left to right).
Robust, $\sigma = 10.0$
Perona-Malik Exponential, K = 10
Perona-Malik Inverse, K = 10

3. EXPERIMENTS

3.1 Test data

To demonstrate the benefit of denoising HRSC images four orbits have been selected. Orbit h2315_0000 has been chosen which was taken at a time and place where the atmosphere was very dusty. Because of a very low signal-to-noise ratio too few tie points have been found and the result of the BA did not fulfil our quality criteria. Figure 3 shows a cutout from the nadir image displayed with a Gaussian stretch.

To illustrate the low contrast of that part Figure 4 shows the histogram and some statistics of the part shown in Figure 3. The very limited grey value range is visible but even weaker areas can be found in the image.

Orbit h1235_0001 was chosen because it contains a lot of noise which does not seem to stem from dust in the atmosphere. h2405_0009 has also very low contrast and the footprint on the surface of Mars contains many homogeneous areas. Nevertheless the result of the BA of this orbit was stated as successful. As a comparison orbit h2032_0001 has been investigated which yields good image quality. In some areas overexposure and compression artefacts are visible. In Table 1 some statistics are given for the entire nadir images.
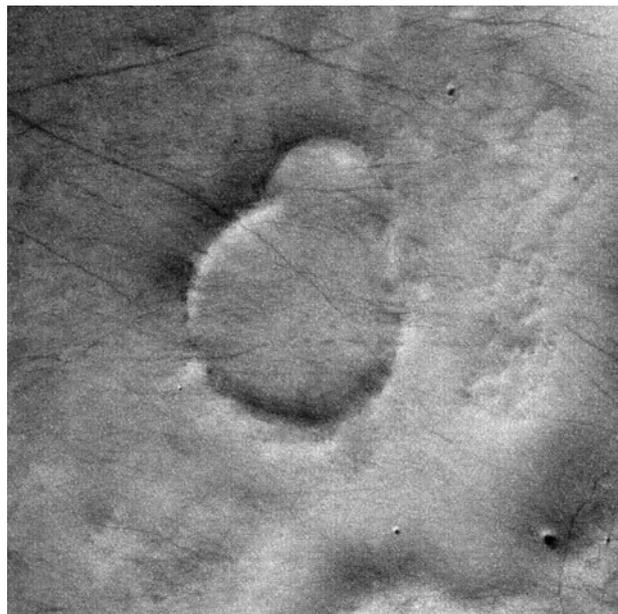
Figure 3: Cutout of 1.000×1.000 pixels from h2315_0000. A Gaussian stretch has been applied.
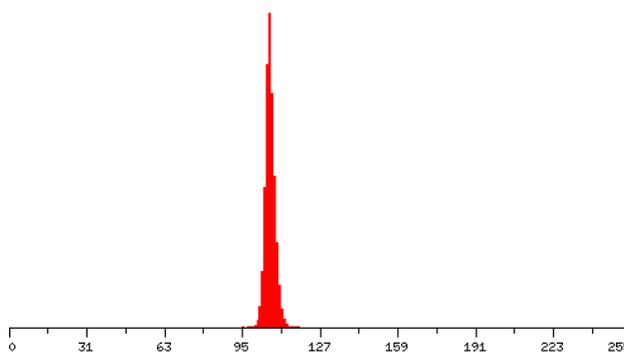
Figure 4: Histogram of Figure 3.
Average Grey Level = 116.1929
Standard Deviation = 2.693420
Min. DN = 103   Max. DN = 128

Orbit	Average	Std. Dev.	MAD	Min	Max
h1235_0001	55.9	10.8	3.0	21	128
h2032_0001	190.9	14.1	4.4	100	292
h2315_0000	105.8	8.3	3.0	63	185
h2405_0009	91.6	8.8	3.0	54	143

Table 1. Image statistics of the chosen test orbits.

3.2 Results

Tie point matching (Heipke et al., 2004) was carried out with smoothed images using the nadir and the two stereo channels of the sensor. In several tests with HRSC imagery it has been found that generally on denoised images more tie points can be extracted. This is helpful since the BA needs a large amount of corresponding points to tie the orbit correctly to the MOLA DTM (Ebner et al., 2004). During these tests it has been found that the MAD is a good estimate of the noise level in the image. However, smoothing was not satisfactorily effective because

only a few more tie points could be derived. A more practical value for the scale has been found with the standard deviation of the image which is higher than the MAD (see also Table 1). Figure 5 shows an enlarged part of the area from Figure 3. Again, to make details visible in the image a Gaussian stretch has been applied. The same area as in Figure 5 after restoration with robust anisotropic diffusion is shown in Figure 6. The noise has been suppressed without blurring the edges.

Figure 5: Part of the original image before restoration.
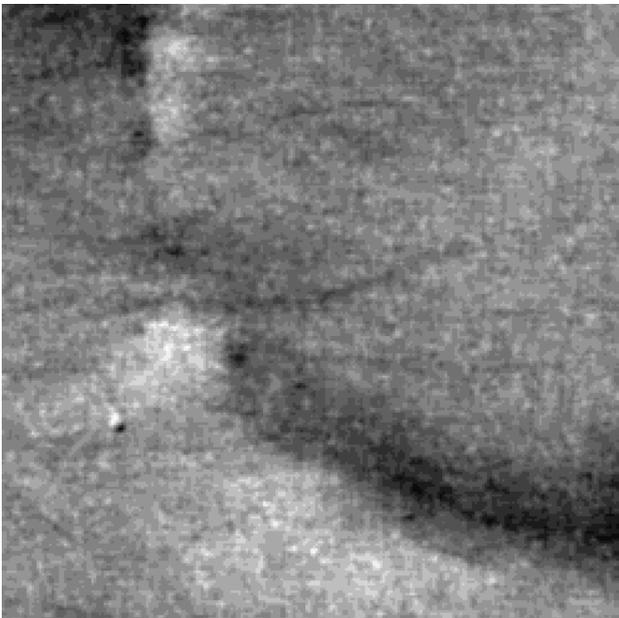
Figure 6: Part of the restored image. Robust anisotropic diffusion with local scale estimate was used.

In Table 2 the number of extracted tie points using the original images and the denoised images is shown. The distribution of the tie points in orbit 2315 before and after denoising is shown in the plot of Figure 7. As can be seen many areas without tie points in the original image could be covered.

Orbit	Original		Denoised	
	2-fold	3-fold	2-fold	3-fold
h1235_0001	4 964	2 712	3 884	5 756
h2032_0001	1 750	7 921	258	9 454
h2315_0000	3 940	1 709	4 555	7 113
h2405_0009	3 853	1 230	7 988	6 568

Table 2. Number of generated tie points before and after filtering.
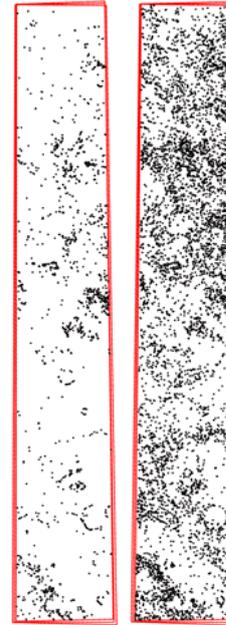
Figure 7: Plot of the distribution of the tie points. Only 3-fold points are shown.

The standard deviations of the ray intersections are not presented here because they could not be improved. However, the improvement of the accuracy of the image coordinates was not anticipated. Table 3 shows the theoretical standard deviations of the biases from BA. A bias in X means a shift of the entire orbit in flight direction, Y across flight direction and Z in height. The biases of the three angles denote: φ = pitch, ω = roll, κ = yaw. Also a drift in Z (a tilt of the orbit in flight direction) was estimated which is not shown here. The actual biases are not shown here because they depend on the a priori accuracy of the EO, topography and altitude of the spacecraft.

Orbit	σ X	σ Y	σ Z	σ φ	σ ω	σ κ
1235	19.2	28.2	7.4	0.3	2.3	0.1
	14.3	21.3	5.6	0.2	1.7	0.1
2032	51.0	37.4	6.8	0.1	1.7	0.1
	50.1	35.1	6.7	0.1	1.7	0.1
2315	114.2	87.6	14.8	0.5	4.9	0.1
	43.1	34.5	6.3	0.2	2.4	0.1
2405	54.5	54.7	12.3	0.6	4.7	0.1
	23.4	21.8	5.5	0.4	2.2	0.1

Table 3. Theoretical standard deviations of biases in meters and milligon respectively. The first line of each orbit is obtained from the original images, the second line from the denoised images.

The table shows that with growing point density the accuracy of the results grows although only minimal improvements could

be achieved in case of orbit 2032. Because of the good image quality of this orbit the increase of point number was small. For orbit 1235 a considerable amount of points could be obtained after denoising and the standard deviation of the biases could be improved. Regarding the other two orbits the standard deviation of the biases could be improved by a factor of 2–3. As expected, the determination of the height offset is more accurate than the lateral shift.

4. CONCLUSIONS

In this paper a brief introduction to anisotropic diffusion and the relationship to robust statistics were given. The work was motivated to obtain more conjugate points with image matching in noisy imagery. It has been shown that more tie points could be obtained by restoring noisy images with robust anisotropic diffusion with a global scale estimate.

Besides the scale another critical parameter has to be set: The number of iterations is important in terms of processing time and restoration effect. For that reason it is not practical to set it to a high value and let the diffusion converge to a constant value. In Mrázek & Navara (2003) the authors give a solution for noise to be removed which is uncorrelated with the signal. Another effect with ascending iterations is that smooth regions can be turned into many segmentation-like regions with no grey value variation. This phenomenon has been observed especially in HRSC images with very low contrast. Higher order nonlinear diffusion can circumvent this problem (Didas et al., 2005). In future work the authors will also investigate the performance of anisotropic diffusion for the derivation of DTMs.

5. REFERENCES

Acton, S. T., 2000. Locally monotonic diffusion. *IEEE Trans. Signal Processing*, (48) 5, pp. 1379–1389.

Barash, D., 2005. Nonlinear Diffusion Filtering on Extended Neighborhood. *Appl. Numer. Math.*, (52) 1, pp. 1–11.

Black, M. J., Sapiro, G., Marimont, D. H., Heeger, D., 1998. Robust Anisotropic Diffusion. *IEEE Trans. Image Processing,* (7) 3, pp. 421–432.

Black, M. J., Sapiro, G., 1999. Edges as Outliers: Anisotropic Smoothing using Local Image Statistics. *In: M. Nielsen et al. (Eds.): Scale-Space'99, Lect. Notes Comput. Sci.*, (1682), pp. 259–270.

Chicarro, A., Martin, P., Trautner, R., 2004. The Mars Express Mission: An Overview. *ESA Special Publications*, SP-1240.

Didas, S., Weickert, J., Burgeth, B., 2005: Stability and Local Feature Enhancement of Higher Order Nonlinear Diffusion Filtering. *In: W. Kropatsch, R. Sablatnig, and A. Hanbury (Eds.): DAGM 2005, LNCS 3663*, pp. 451–458.

Ebner, H., Spiegel, M., Baumgartner, A., Giese, B., Neukum, G., and the HRSC Co-Investigator Team, 2004. Improving the Exterior Orientation of Mars Express HRSC Imagery. *IntArchPhRS*, (35) 4, pp. 852–857.

Gwinner, K., Scholten, F., Giese, B., Oberst, J., Jaumann, R., Spiegel, M., Schmidt, R., Neukum, G., 2005. Hochauflösende Digitale Geländemodelle der Marsoberfläche auf der Grundlage von Mars Express HRSC Daten. *Photogrammetrie Fernerkundung Geoinformation (PFG)*, (5), pp. 387–394.

Hampel, F.R., 1974. The Influence Curve and its Role in Robust Estimation. *J. Am. Stat. Assoc.*, (69) 364, pp. 383–393.

Hampel, F. R., Ronchetti, E. M., Rousseeuw, P. J., Stahel, W. A., 1986. *Robust Statistics: The Approach Based on Influence Functions.* Wiley, New York.

Heipke, C., Schmidt, R., Brand, R., Oberst, J., Neukum, G. and the HRSC Co-Investigator Team, 2004. Performance of Automatic Tie Point Extraction using HRSC Imagery of the Mars Express Mission. *IntArchPhRS*, (35) 4, pp. 846–851.

Koenderink, J J., 1984. The Structure of Images. *Biol. Cybern.*, (50) 5, pp. 363–370.

Leclerc, Y. G., 1989. Constructing Simple Stable Descriptions for Image Partitioning. *Int. J. Computer Vision*, (3) 1, pp. 73–102.

Mrázek, P, Navara, M., 2003. Selection of Optimal Stopping Time for Nonlinear Diffusion Filtering. Int. J. Computer Vision, (52) 2/3, pp. 189–203.

Neukum, G., Jaumann, R. and the HRSC Co-Investigator Team, 2004. HRSC: The High Resolution Stereo Camera of Mars Express. *ESA Special Publications*, SP-1240.

Perona, P., Malik, J., 1990. Scale-space and Edge Detection using Anisotropic Diffusion. *IEEE Trans. Pattern Analysis and Machine Intelligence*, (12) 7, pp. 629–639.

Rousseeuw, P. J., Bassett, G. B. Jr., 1990. The Remedian: A Robust Averaging Method for Large Data Sets. *J. Am. Stat. Assoc.*, (85) 409, pp. 97–104.

Scholten, F., Gwinner, K., Roatsch, T., Matz, K.-D., Wählisch, M., Giese, B., Oberst, J., Jaumann, R., Neukum, G. and the HRSC Co-Investigator Team, 2005. Mars Express HRSC Data Processing – Methods and Operational Aspects. *PE&RS*, (71) 10, pp. 1143–1152.

Witkin, A. P., 1983. Scale-Space Filtering. *Proc. Int. Joint Conf. Artificial Intelligence*, Karlsruhe, pp. 1019–1021.

Zuber, M. T., Smith, D. E., Solomon, S. C., Muhleman, D. O., Head, J. W., Garvin, J. B., Abshire, J. B., Bufton, J. L., 1992. The Mars Observer Laser Altimeter Investigation. *J. Geophys. Res.*, (97) E5, pp. 7781–7797.

6. ACKNOWLEDGEMENTS